Research article

Choloong Hahn, Akram Hajebifard and Pierre Berini*

Helium focused ion beam direct milling of plasmonic heptamer-arranged nanohole arrays

https://doi.org/10.1515/nanoph-2019-0385
Received September 24, 2019; revised November 5, 2019; accepted November 9, 2019

Abstract: We fabricate plasmonic heptamer-arranged nanohole (HNH) arrays by helium (He) focused ion beam (HeFIB) milling, which is a resist-free, maskless, direct-write method. The small He^+ beam spot size and high milling resolution achieved by the gas field-ionization source used in our HeFIB allows the milling of high aspect ratio (4:1) nanoscale features in metal, such as HNHs incorporating 15 nm walls of high verticality between holes in a 55-nm-thick gold film. Drifts encountered during the HeFIB milling of large arrays, due to sample stage vibrations or He beam instability, were compensated by a drift correction technique based on *in situ* He ion imaging of alignment features. Our drift correction technique yielded 20 nm maximum dislocation of HNHs, with 6.9 and 4.6 nm average dislocations along the horizontal and vertical directions, respectively. The measured optical resonance spectra of the fabricated plasmonic HNH arrays are presented to support the fabrication technique. Defects associated with HeFIB milling are also discussed.

Keywords: focused ion beam; helium ion microscopy; nanofabrication; plasmonics.

***Corresponding author: Pierre Berini,** School of Electrical Engineering and Computer Science, University of Ottawa, Ottawa K1N6N5, Canada; Center for Research in Photonics, University of Ottawa, Ottawa K1N6N5, Canada; and Department of Physics, University of Ottawa, Ottawa, Ottawa K1N6N5, Canada, e-mail: pberini@uottawa.ca
Choloong Hahn: School of Electrical Engineering and Computer Science, University of Ottawa, Ottawa K1N6N5, Canada; and Center for Research in Photonics, University of Ottawa, Ottawa K1N6N5, Canada. https://orcid.org/0000-0003-3213-345X
Akram Hajebifard: Center for Research in Photonics, University of Ottawa, Ottawa K1N6N5, Canada; and Department of Physics, University of Ottawa, Ottawa, Ottawa K1N6N5, Canada

1 Introduction

Nanofabrication technologies have attracted great interest due to the possibilities of opening new functionalities by structuring materials at the nanoscale or creating devices of extremely small size. One of the most common and popular approaches to nanofabrication consists of using electron beam lithography (EBL), which can cover feature sizes from the microscales to the nanoscales by overlay or using complementary beam parameters [1]. Various photonic devices have been successfully realized with EBL, including plasmonic distributed feedback lasers [2], non-Hermitian photonic devices [3], and plasmonic nanoantennas to enhance high harmonic generation [4]. FIB milling using gallium (Ga) ions is also a very common approach to nanofabrication [5–7]. However, it is limited in resolution and may produce significant material redeposition and undesired implantation of ions into the substrate [8].

The development of gas field-ionization source technology allows helium (He) to be used as the ion beam. An HeFIB can have a beam spot size of less than 0.5 nm [9] and a direct milling resolution of 3.5 nm [10] due to the atomically defined metal tip used to form the He beam and the small de Broglie wavelength of He ions. Unlike liquid metal ion sources, such as Ga, He ions are pulled by high extraction voltages from a sharp, atomically defined metal tip, so they have a higher axial directionality, enabling high aspect ratio features to be defined by HeFIB direct milling [11, 12]. In addition, He ions produce less contamination by unintentional implantation, as He is a noble gas, and it has a high propensity to diffuse out of materials [13]. HeFIB milling is also more controllable due to the slow milling rate caused in part by the low atomic weight of He, making HeFIB milling more suitable for the controlled milling of sub-20 nm features [14]. Although a novel technique, HeFIB milling has already been applied to nanofabrication in several materials, such as graphene [15, 16], silicon nitride [17], and Au [18], including the fabrication of plasmonic antennas with partially loaded nanogaps [19].

Arrays of nanoholes in a metal film produce field enhancement and resonances that can be tuned over

a wide spectral range, motivating applications in, for example, surface-enhanced Raman scattering [20] and optical biosensors [21, 22]. Heptamer-arranged nanoholes (HNHs) are hexagonal close-packed arrangements of seven nanoholes in a metal film, inspired by complementary arrangements of metal nanoparticles [23]. Arrays of HNHs in a metal film are very interesting for their highly complex, rich spectral responses and pronounced Fano resonances involving propagating surface plasmon polaritons (SPPs), localized SPPs (LSPPs), and Wood's anomaly (WA) waves [24]. However, the fabrication of HNH arrays in a metal film is very challenging due to the small distance between the holes required for close-packing (10–15 nm) and the commensurate need for high verticality sidewalls in a 30- to 60-nm-thick metal film [24]; that is, nanoscale features with a 4:1 aspect ratio are required. Here, we report novel techniques developed using HeFIB milling of an Au film to form high-quality arrays of HNHs and demonstrate the operation of the arrays via optical measurements.

2 Fabrication

A unit cell of the HNH array of interest in this paper is illustrated in Figure 1A. An HNH arrangement consists of seven close-packed nanoholes in an Au film on an SiO_2 substrate. The geometrical parameters, including the diameter of each nanohole (D), the interhole separation (G), the periodicity of the array (P), and the thickness of the Au film (T), are chosen according to the desired spectral range of the resonances. Here, we chose $D = 100$ nm, $G = 15$ nm, $P = 480$ nm, and $T = 55$ nm for application in the near-infrared spectral region [24]. Figure 1B shows the He ion microscope (HIM) images in tilted (54°) and top views of HNHs in a 55-nm-thick Au film taken after direct milling via HeFIB. The quality of the structures is evidently high: sharp edges are observed, the sidewalls are rather vertical, no milled material seems to be redeposited, and the dimensions achieved are accurate. A benefit of the HeFIB is that the same He ion source can be used for *in situ* microscopy and imaging via the detection of secondary electrons by simply adjusting the dose delivered to the sample. However, He microscopy is a destructive imaging method even at low He doses, so exposure to the He beam should be minimized to protect the sample surface from undesired damage.

For direct HeFIB milling, an SiO_2 substrate (fused silica) was coated by a 0.3-nm-thick layer of Cr as an adhesion layer followed by a 55-nm-thick Au layer. The Au layer was deposited by thermal evaporation at a rate of 0.5 Å s^{-1}, whereas the Cr layer was deposited by electron beam evaporation at a rate of 0.1 Å s^{-1}. All layers were deposited sequentially without breaking vacuum using an Angstrom NEXDEP evaporator. No protective layer on the Au surface was used in this process. Our Au deposition process targeted 60 nm in thickness, but we achieved 55 nm as measured by atomic force microscopy on a witness sample.

The prepared layered stacks were milled to create 20×20 arrays of HNHs using an HeFIB system (Zeiss Orion NanoFab) controlled using the nanopatterning and visualization engine (NPVE). In direct milling, the final structure is ready for use immediately after milling without any subsequent wet processes. An HIM image of an Au HNH array fabricated by direct HeFIB milling is shown in Figure 2A.

The He ion beam was prepared in an He gas pressure of 5×10^{-6} Torr using a 10 μm aperture diameter and a spot

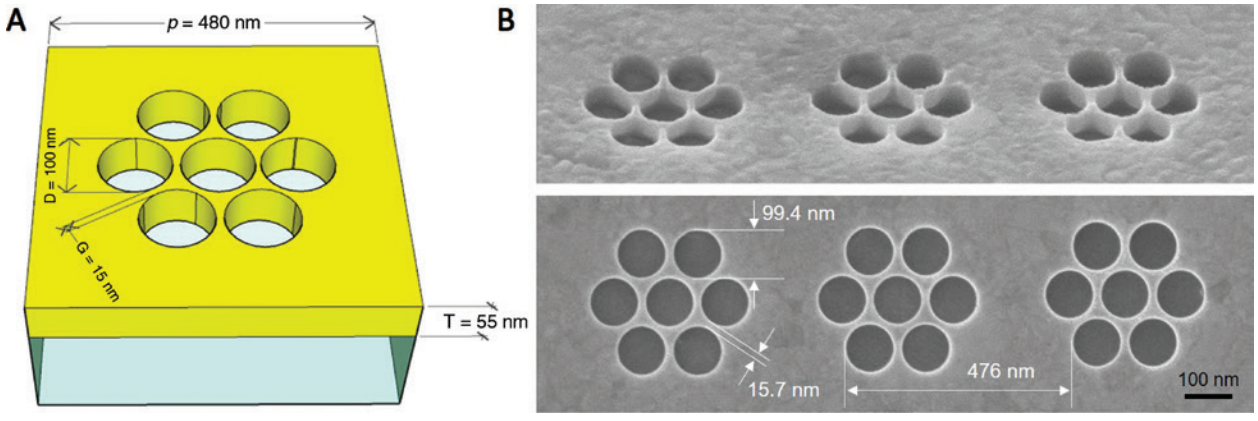

Figure 1: HNH array in an Au film.
(A) Schematic of the HNH design with the target dimensions. The Au film (yellow) is 55 nm thick and is supported by an SiO_2 (fused silica) substrate (light blue). (B) HIM images of HNHs fabricated via direct HeFIB milling. Top, 54° tilted view; bottom, top view.

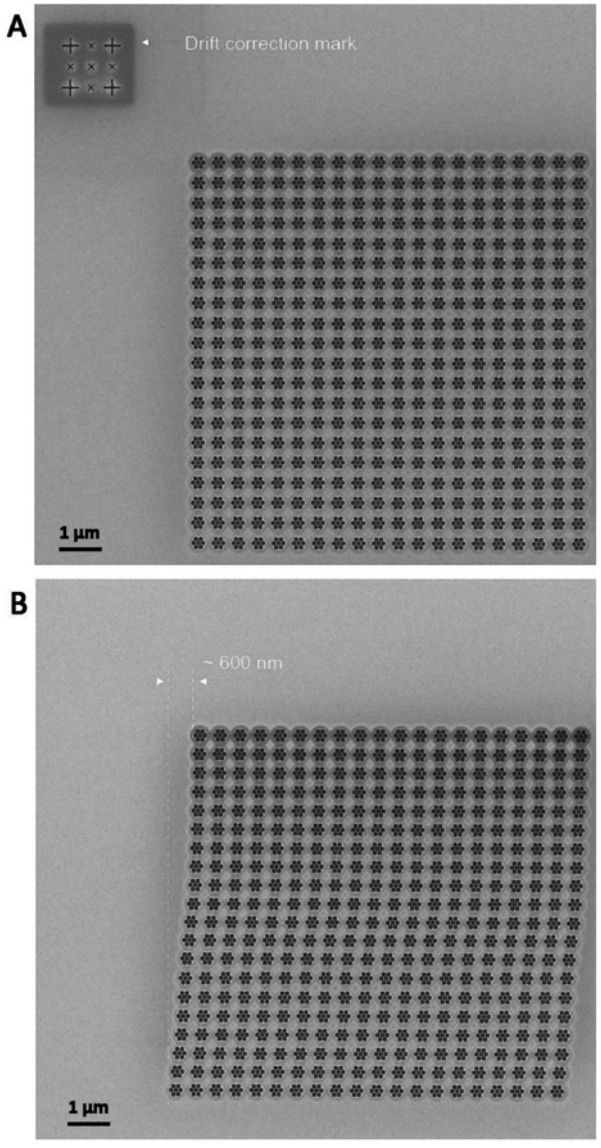

Figure 2: HIM images of 20 × 20 arrays of Au HNHs.
(A) Array fabricated with drift correction. (B) Array fabricated without drift correction.

control parameter of 3.5, which resulted in a 10 pA He ion beam current using a 25 keV acceleration voltage. Here, the spot control parameter refers to the setting on the condenser lens, which focuses the beam through the aperture and affects the directionality of the beam. A single HNH was milled via a double-serpentine exposure method with 1 µs dwell time, 0.25 nm pixel spacing, and several repeats to achieve the target dose. Double-serpentine exposure is applied as in a serpentine scan; however, instead of going back to the first dwell point once the first frame is completed, the same pattern is scanned but in the reverse direction. In this manner, the horizontal and vertical refresh times are ignored, yielding efficient patterning in time. The layout for a single HNH was prepared as a single shape by the union of seven circles to ensure that all holes would be exposed within one iteration. Clearing doses to the substrate were initially estimated by *in situ* endpoint detection and subsequently confirmed by measured optical responses (discussed below). The clearing doses were found to be 10 nC μm^{-2} for the 55-nm-thick Au layer in the direct HeFIB milling process. Endpoint detection is a built-in function of NPVE, which captures live intensity images via secondary electron emission during milling. This is useful for the initial estimation of the clearing dose of each layer and is rather accurate especially when the milled material changes from conductive to insulating or vice versa.

He ions have low atomic weight, which leads to advantages in HeFIB milling such as the ability to define very fine features with a high degree of control over the milling process. However, a drawback is that the sputtering yield of an HeFIB process can be very low, leading to long milling times. For instance, the fabrication of a 20 × 20 array of HNHs requires a writing time of about 3 h. Our HeFIB system drifts over such a period of time, due to either stage drift or beam instability, resulting in skewed arrays. For this reason, drift correction was applied after the completion of every five HNH structures by imaging predefined features, calculating the drift from the image, and compensating in subsequent millings. The drift correction mechanism is a built-in function of the NPVE software used for HeFIB patterning. Here, we used several premilled crosses as shown in Figure 2A (top left) for drift correction. Figure 2B shows an HIM image of a 20 × 20 HNH array milled without drift correction, revealing that about 600 nm of lateral drift occurred during milling of the array. Figure 2A shows an image of an array written with drift correction, which effectively compensated for instrument drift.

We used a combination of several crosses of different sizes and shapes as the drift correction marks for better recognition and placed them ~3 µm away from the top left corner of the HNH array. This location was chosen far enough to avoid any damage to the array while exposing the drift correction marks to He ions during imaging yet close enough to avoid any mechanical stage movement by keeping the marks within the small field of view required to ensure high-resolution milling. As the drift correction is based on a destructive imaging method (He ion irradiation), the number of corrections allowed while milling one array is limited and dependent on the imaging parameters used. Also, there is a trade-off between the frequency and the accuracy of drift correction because high-resolution imaging is more destructive. Here, we achieved a maximum dislocation of HNHs of less than 20 nm for

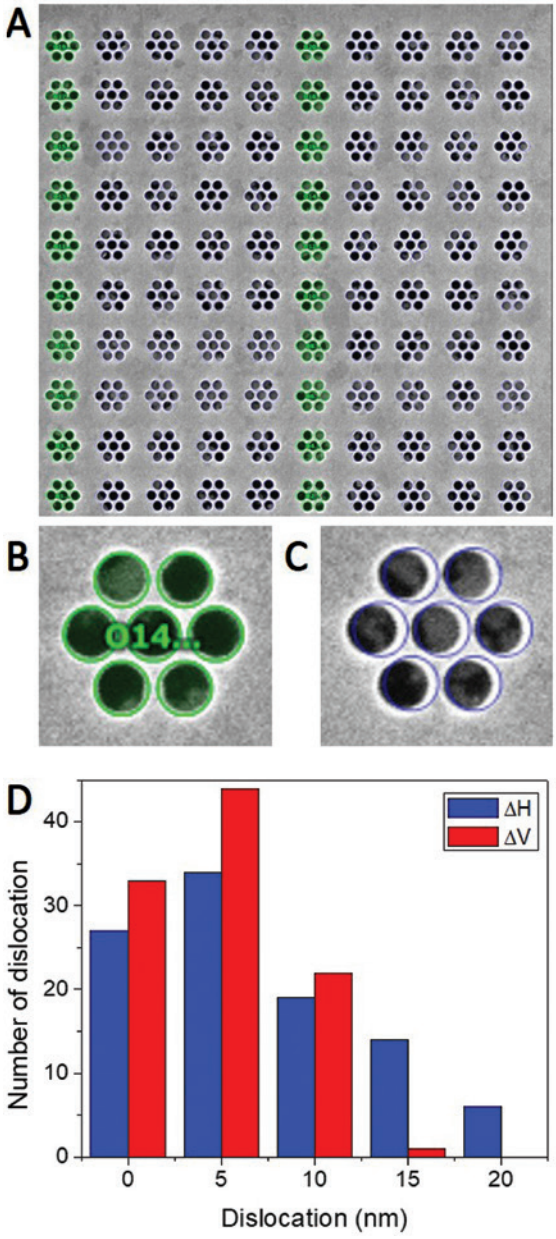

Figure 3: Dislocation of HNHs with drift correction.
(A) HIM image of fabricated HNH array overlapped with the patterning layout. Digital zoomed-in image of a single HNH for (B) $\Delta H = \Delta V = 0$ and (C) $\Delta H = 20$ nm and $\Delta V = 5$ nm. (D) Distribution of dislocations in the horizontal (ΔH) and vertical (ΔV) directions for each HNH in an array.

most of the fabricated arrays using a 6.3 nm pixel spacing and 1 µs dwell time while imaging for drift correction. We avoided the destruction of the predefined correction marks, although Figure 2A reveals a shallow milled-out area around the marks due to repeated imaging.

The dislocations of each HNH fabricated with drift correction was measured from an HIM image of the fabricated HNHs overlapped with the layout pattern, as shown in Figure 3A. The blue and green colored circles are the layout pattern, and the green circles with an object label indicate the location in the array where the drift correction was applied. To collect enough HNHs for statistical analysis, we used an image of a 10×10 array at 1024×1024 pixel resolution, which results in a 5 nm pixel spacing. Figure 3B and C shows the digital zoomed-in images of Figure 3A as examples of a single HNH without dislocation and of one with horizontal dislocation ($\Delta H = 20$ nm) and vertical dislocation ($\Delta V = 5$ nm), respectively. The dislocations measured in Figure 3A are plotted in Figure 3D as the number of dislocations. The average dislocations in both directions are obtained as $\Delta H_{AVE} = 6.9$ nm and $\Delta V_{AVE} = 4.6$ nm with 20 and 15 nm maximum horizontal and vertical dislocations, respectively.

3 Discussion

The optical transmittance response was measured for several fabricated plasmonic HNH arrays. A tunable Ti:sapphire laser (SpectraPhysics) was used as the light source that delivers a highly coherent continuous-wave (CW) output ranging from 700 to 980 nm. With the assistance of a custom microscope operating in the visible range and integrated into the optical path, a vertically polarized light beam was focused onto the sample surface to a 10 µm spot size and positioned at the center of an HNH array. The power spectral response of the sample was measured in transmission relative to a reference power (for noise suppression) followed by the response of the set-up without the sample also relative to a reference power, and the transmittance of the sample was taken as the ratio of these power spectral responses.

The measured optical transmittance spectra of HNH arrays fabricated with doses of 8, 10, and 12 nC µm^{-2} are given in Figure 4A–C, respectively. The corresponding scanning electron microscopy (SEM) image of the array associated with the black response in each plot is also given. The array fabricated with a dose of 10 nC µm^{-2}, which is the clearing dose estimated by endpoint detection, produces a clear resonance spectrum as shown in Figure 4B (black solid curve). The optical transmittance of an HNH array with the same structural parameters as the fabricated one was calculated for vertical linearly polarized incident light, as shown in Figure 5A. As discussed in our previous work [24], an HNH array can support several excitations, including propagating SPPs due to the periodicity of the array, LSPPs resonating on HNHs, and WA waves. Unlike our previous work [24], where the HNH array had $G = 10$ nm and was covered by a dielectric material of refractive index $n_s = 1.33$, here we have

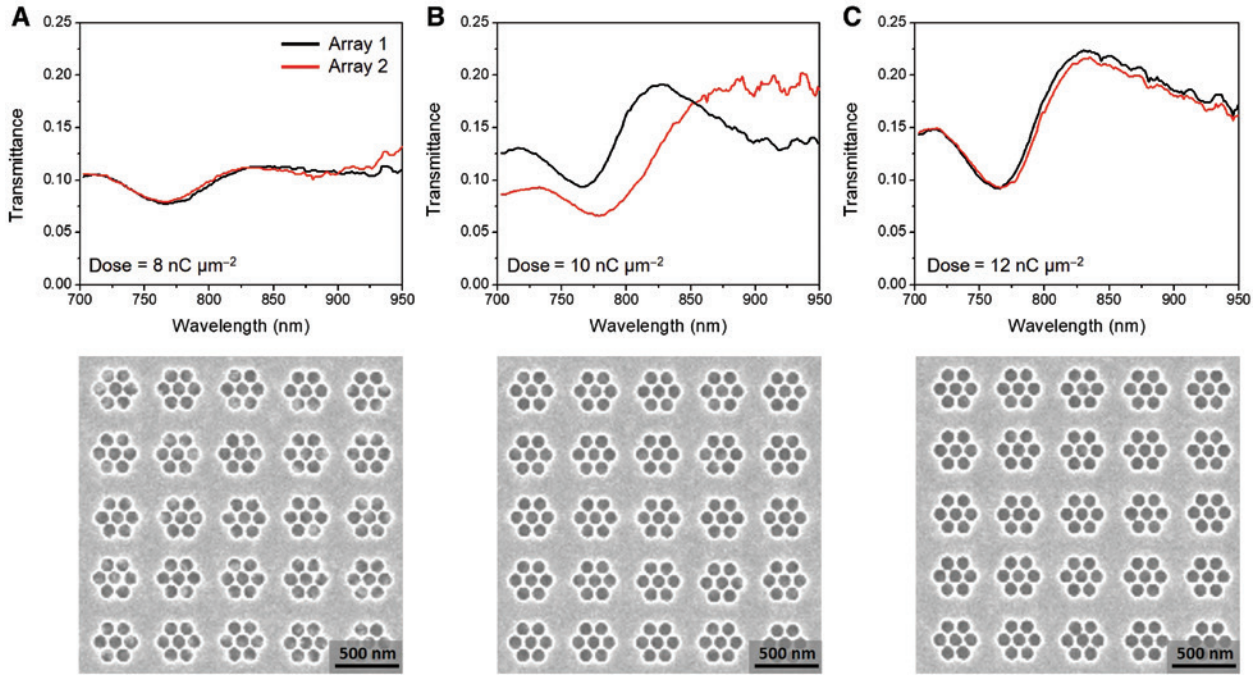

Figure 4: Optical transmittance responses (top) and SEM images (bottom) of HNH arrays fabricated by direct HeFIB milling at the milling dose of (A) 8 nC μm^{-2}, (B) 10 nC μm^{-2}, and (C) 12 nC μm^{-2}.
The black and red curves are measurements for repeated fabrication iterations.

$G = 15$ nm and $n_s = 1$. Increasing G and decreasing the superstrate refractive index n_s result in a blue shift of the resonant wavelengths. Here, the LSPP and SPP peaks in the transmittance spectrum occur at 810 and 710 nm, respectively, which are blue shifted from 905 and 782 nm (respectively) in comparison to our previous work. The WA-SPP resonance no longer exists in the present system because the condition to support this resonance is no longer satisfied when the array is covered by air. As observed in Figure 4A, the second resonance peak, corresponding to LSPPs (~810 nm), disappears at the lower dose because the nanoholes are not milled out completely through the Au layer, so they cannot support strong LSPP resonances. This is also observed in the SEM image of Figure 4A (bottom), which shows the residual material at the bottom of the nanoholes. Increasing the milling dose from 8 nC μm^{-2} (Figure 4A) to 10 nC μm^{-2} (Figure 4B), results in an array of nanoholes, which does not have any Au residue in the holes and thus produces a profound LSPP resonance in its optical transmittance response (~810 nm). By increasing the dose to 12 nC μm^{-2} (Figure 4C), the broadening of the LSPP resonance is observed, which implies breaking or degradation in the metal walls between nanoholes, although this is not clearly recognizable in the SEM image.

The black and red curves in Figure 4 correspond to the optical transmittance responses of two different arrays fabricated with identical parameters. The overlap in their optical responses is indicative of the repeatability of the HeFIB direct milling process. Good repeatability is observed in the case of the arrays of Figure 4A and C. However, the red and black curves in Figure 4B do not coincide well. For the array corresponding to the red curve in Figure 4B, our drift correction scheme failed as can be appreciated from the He microscope image of this array taken immediately after milling, as shown in Figure 5B. In Figure 5B, we overlap the layout in blue on the image to show the mismatch between the layout and the fabricated array (the poor quality of this image is intended to protect the fabricated array from damage caused by He ion beam imaging). Our drift correction scheme can occasionally fail if low-quality imaging is carried out during drift correction, which rarely happened over many milling trials. As mentioned earlier, there is a trade-off between imaging quality for drift correction and the number of allowed drift correction steps. Due to this limitation, we achieved about 80% production yield of HNH arrays.

An alternative approach to FIB milling is metal-assisted FIB (MA-FIB) milling, which uses a metallic protective layer on top of the target layer [25]. The main purpose of using a protective layer in MA-FIB milling is to prevent blunt edges and protect the device surface against redeposition of milled material onto the surface. It is shown in the images in Figure 1B that direct HeFIB milling of an Au film produces nanoholes with sharp edges and

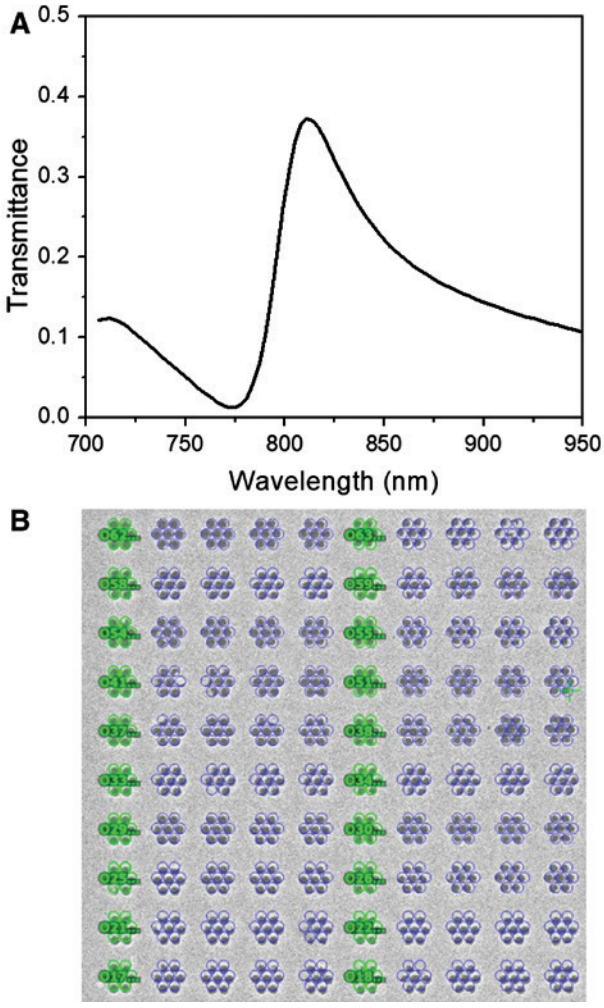

Figure 5: Theoretical calculation and drift correction failure. (A) Theoretical optical transmittance response of an HNH array. (B) HIM image overlapped with layout pattern, indicating drift correction failure.

dimensions that are very close to target. This is due to the high directionality of the He ion beam used for machining. Also, no major redeposition of milled material can be observed in these images likely due to the low sputtering yield of light He ions. Therefore, although useful in milling with heavier ions (e.g. Ga), a protective layer seems unnecessary for HeFIB milling, especially under the conditions explored herein.

4 Conclusions

In summary, we presented the fabrication of plasmonic HNH arrays using an HeFIB direct milling process. A drift correction scheme based on periodic He imaging of alignment marks was also devised and demonstrated to be very effective in countering instrument drift. Arrays of 20×20 HNHs were successfully fabricated via direct milling HeFIB, in a 55-nm-thick Au layer, on an SiO_2 substrate, where each HNH consisted of seven close-packed holes, each 100 nm in diameter and separated by 15 nm edge-to-edge; high aspect ratio nanoscale features (4:1) were therefore achieved. Direct milling HeFIB produces high-quality HNHs with sharp edges and no milled material redeposition due to the high directionality and light atomic mass of He ions. The use of a protective layer was therefore deemed unnecessary under the milling conditions applied. The optical transmittance response of fabricated HNH arrays confirmed the proper operation of the structures in the near-infrared, with SPP resonances localized to HNHs being evident. Direct HeFIB milling yields high-quality nanostructures with minimal milled material redeposition, but the milling rates are low, so a drift correction scheme is necessary to counter instrument drift if large milled areas are required. The technique also involves minimal solvent and material contact and has the potential to be applied broadly to the investigation of plasmonic nanohole and nanoparticle arrays of different shapes and arrangements.

References

[1] Fong NR, Berini P, Tait N. Fabrication of long-range surface plasmon hydrogen sensors on Cytop membranes integrating grating couplers. J Vac Sci Technol B 2015;33:021201.
[2] Karami Keshmarzi E, Tait RN, Berini P. Single-mode surface plasmon distributed feedback lasers. Nanoscale 2018;10:5914–22.
[3] Yoon JW, Choi Y, Hahn C, et al. Time-asymmetric loop around an exceptional point over the full optical communications band. Nature 2018;562:86–90.
[4] Vampa G, Ghamsari BG, Siadat Mousavi S, et al. Plasmon-enhanced high-harmonic generation from silicon. Nat Phys 2017;13:659–62.
[5] Tseng AA. Recent developments in nanofabrication using focused ion beams. Small 2005;1:924–39.
[6] Vesseur EJR, De Abajo FJG, Polman A. Modal decomposition of surface plasmon whispering gallery resonators. Nano Lett 2009;9:3147–50.
[7] Lanyon YH, De Marzi G, Watson YE, et al. Fabrication of nanopore array electrodes by focused ion beam milling. Anal Chem 2007;79:3048–55.
[8] Ocelic N, Hillenbrand R. Subwavelength-scale tailoring of surface phonon polaritons by focused ion-beam implantation. Nat Mater 2004;3:606–9.
[9] Marshall MM, Yang J, Hall AR. Direct and transmission milling of suspended silicon nitride membranes with a focused helium ion beam. Scanning 2012;34:101–6.
[10] Scholder O, Jefimovs K, Shorubalko I, Hafner C, Sennhauser U, Bona G-L. Helium focused ion beam fabricated

plasmonic antennas with sub-5 nm gaps. Nanotechnology 2013;24:395301.
[11] Seniutinas G, Gervinskas G, Anguita J, Hakobyan D, Brasselet E, Juodkazis S. Nano-proximity direct ion beam writing. Nanofabrication 2015;2:54–62.
[12] Scipioni L, Ferranti DC, Smentkowski VS Potyrailo RA. Fabrication and initial characterization of ultrahigh aspect ratio vias in gold using the helium ion microscope. J Vac Sci Technol B 2010;28:C6P18–23.
[13] Kollmann H, Piao X, Esmann M, et al. Toward plasmonics with nanometer precision: Nonlinear optics of helium-ion milled gold nanoantennas. Nano Lett 2014;14:4778–84.
[14] Wang Y, Boden SA, Bagnall DM, Rutt HN, De Groot CH. Helium ion beam milling to create a nano-structured domain wall magnetoresistance spin valve. Nanotechnology 2012;23:395302.
[15] Lemme MC, Bell DC, Williams JR, et al. Etching of graphene devices with a helium ion beam. ACS Nano 2009;3:2674–6.
[16] Kalhor N, Boden SA, Mizuta H. Sub-10 nm patterning by focused He-ion beam milling for fabrication of downscaled graphene nano devices. Microelectron Eng 2014;114:70–7.
[17] Emmrich D, Beyer A, Nadzeyka A, et al. Nanopore fabrication and characterization by helium ion microscopy. Appl Phys Lett 2016;108:163103.
[18] Melli M, Polyakov A, Gargas D, et al. Reaching the theoretical resonance quality factor limit in coaxial plasmonic nanoresonators fabricated by helium ion lithography. Nano Lett 2013;13:2687–91.
[19] Wang Y, Abb M, Boden SA, et al. Ultrafast nonlinear control of progressively loaded, single plasmonic nanoantennas fabricated using helium ion milling. Nano Lett 2013;13:5647–53.
[20] Liu Z, Ye J. Highly controllable double Fano resonances in plasmonic metasurfaces. Nanoscale 2016;8:17665–74.
[21] Brolo AG, Gordon R, Leathem B, Kavanagh KL. Surface plasmon sensor based on the enhanced light transmission through arrays of nanoholes in gold films. Langmuir 2004;20:4813–5.
[22] Lesuffleur A, Im H, Lindquist NC, Lim KS, Oh SH. Laser-illuminated nanohole arrays for multiplex plasmonic microarray sensing. Opt Express 2008;16:219–24.
[23] Ye J, Wen F, Sobhani H, et al. Plasmonic nanoclusters: near field properties of the Fano resonance interrogated with SERS. Nano Lett 2012;12:1660–7.
[24] Hajebifard A, Berini P. Fano resonances in plasmonic heptamer nano-hole arrays. Opt Express 2017;25:18566–80.
[25] Kannegulla A, Cheng L. Metal assisted focused-ion beam nanopatterning. Nanotechnology 2016;27:36LT01.